RSC Advances

PAPER

View Article Online
View Journal | View Issue

Cite this: *RSC Adv.*, 2022, **12**, 31293

A novel family of small molecule HIF-1 alpha stabilizers for the treatment of diabetic wounds; an integrated *in silico*, *in vitro*, and *in vivo* strategy†

Esakkimuthukumar M.,[a] Akey Krishna Swaroop,[a] Sunil Kumar Patnaik,[a] Rajesh Kumar R.,[b] Praveen T. K.,[c] Mudavath Ravi Naik[c] and Jubie S. *[a]

Hypoxia-inducible factor-1 alpha (HIF-1α) is a crucial regulator of wound healing, which includes epithelialization, angiogenesis, granulation, tissue development, and wound contraction. Even though diabetic wounds are hypoxic, HIF-1α levels are decreased during healing. Diabetic wound healing necessitates the modulation of hypoxia-induced responses by VHL–HIF-1α protein–protein inhibition. Our proposed hypothesis is to increase HIF-1α levels by inhibiting VHL and HIF-1α interactions by novel small bioactive molecules, accelerating diabetic wound healing. A three features (two aromatic rings and one hydrogen bond acceptor) pharmacophore hypothesis was generated from the existing HIF-1α modulators. Virtual screening was done based on the generated pharmacophore, and a library consisting of the top 20 out of 3728 compounds was selected using ZINCPharmer. Of the top 20 molecules, the pyrazole moiety was identified as the top "HIT". Five analogues of pyrazole were designed, and Scifinder ascertained the novelty. The designed compounds were synthesized and characterized by IR, Mass, and NMR. Preliminarily, we have carried out a scratch wound assay using 3T3L1 cell lines. All the synthesized compounds showed significant wound healing activity. Further, to validate the *in vitro* assay, the compound **CI**, which showed effective *in vitro* results was used for *in vivo* study. Using the diabetes mouse model, comprising streptozotocin-induced (STZ) diabetic mice and scratch wound assay, we demonstrated that inhibiting the VHL and HIF-1α connection is a promising strategy for treating diabetic ulcers. Molecules CI and CP were found to have substantial *in silico*, *in vitro*, and *in vivo* outcomes.

Received 26th August 2022
Accepted 20th October 2022

DOI: 10.1039/d2ra05364k

rsc.li/rsc-advances

1 Introduction

Epithelialization, angiogenesis, granulation, tissue development, and wound contraction are all parts of the systematic and dynamic process of wound healing that are controlled by hypoxia-inducible factor 1 (HIF-1α).[1] Due to oxygen-dependent hydroxylation of HIF-1α by prolyl hydroxylase domain proteins (PHDs), steady-state levels of HIF-1α are low in normal tissues.[2] That enables the tumour suppressor protein Von Hippel-Lindau (VHL) to bind to HIF-1α and form a complex quickly destroyed by the proteasome.[3] Remarkably, hyperglycaemia can reduce HIF-1α′s stability and impede its target genes' expression, which may explain diabetic patients' poor wound healing and ulcer problems.[4] That suggests that improving the stability of HIF-1α, such as by preventing the interaction between VHL and HIF-1α, may be a potential approach for treating wound problems associated with diabetes. PPIs (protein–protein interactions) are desirable targets in the search for new drugs.[5] Recent successes suggest that protein–protein interactions might function more effectively. Targeting the interfaces between interacting proteins for therapeutic purposes is of great interest, ideally using tiny "drug-like" compounds, which are typically less expensive and can be taken orally rather than intravenously.[6] In the current study, we present the discovery of pyrazolo-analogues as a potent inhibitor of the VHL–HIF–1α PPI, which can successfully stimulate the accumulation of HIF-1α.

HIF-1α levels are decreased during healing even though diabetic wounds are hypoxic. The control of hypoxia-induced responses is necessary for diabetic wound healing. HIF-1α and the tumour suppressor protein Von Hippel-Lindau (VHL) combine to form a complex that the proteasome quickly identifies and destroys. That is because oxygen-dependent hydroxylation of HIF-1α by PHD proteins keeps stable HIF-1 levels minimal in healthy tissue. HIF-1α cannot operate normally when blood sugar levels are too high. That could be why ulcers and wounds in people with diabetes heal more slowly and are more likely to happen. Diabetes wound aspects may be

[a]*Department of Pharmaceutical Chemistry, JSS College of Pharmacy, JSS Academy of Higher Education and Research, Ooty, Tamilnadu, India. E-mail: jubie@jssuni.edu.in*
[b]*Department of Pharmaceutical Biotechnology, JSS College of Pharmacy, JSS Academy of Higher Education and Research, Ooty, Tamilnadu, India*
[c]*Department of Pharmacology, JSS College of Pharmacy, JSS Academy of Higher Education and Research, Ooty, Tamilnadu, India*

† Electronic supplementary information (ESI) available. See DOI: https://doi.org/10.1039/d2ra05364k

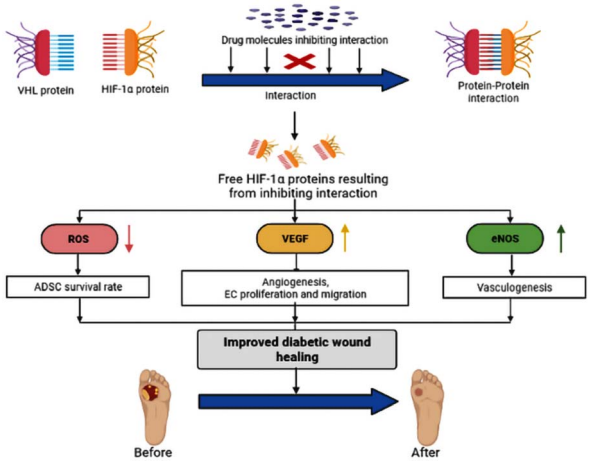

Fig. 1 Proposed hypothesis.

managed by increasing the stability of HIF-1α and working to reduce the interaction between VHL and HIF-1α. To date, the only compound VH298 has been shown to stimulate wound healing and a wide range of activity healing in animals, and there aren't many substances that can block the interaction between VHL and HIF-1α.[7]

Based on the preceding information, our proposed theory is to increase HIF-1α levels by blocking the interactions between VHL and HIF-1α with novel small bioactive molecules, which would help accelerate the healing of diabetic wounds Fig. 1.

(1) ADSC (adipose-derived stem cells) survival rates tend to rise when ROS levels are reduced, which promotes the healing of damaged tissue.[8]

(2) Angiogenesis, epithelial cell migration, and proliferation both increase in response to VEGF levels.[9]

(3) Increase eNOS levels, which trigger vasculogenesis. As a result, it enhances the blood supply to the wound area.[10]

2 Materials and methods

2.1 *In silico* studies

2.1.1 Software used. To generate pharmacophore modelling, virtual screening, ligand preparation, identification of protein, preparation of protein, docking, 2D interaction analysis, novelty checking, ADME and toxicity studies were analyzed by software like PharmaGist, ZINCPharmer, MarvinSketch, Protein Data Bank, Swiss-Pdb Viewer, PyRx 0.9, Discovery Studio Visualizer, Sci-finder, SwissADME, PreADMET respectively.

2.2 Pharmacophore modelling

PharmaGist pharmacophore technique utilizes a circuitous methodology that requires a 3D test set as data. PharmaGist identifies new pharmacophores by using various adaptable arrangements of the test set. PharmaGist strategy comprises four steps: ligand representation, multiple pairwise alignments, clustering, and output. Each ligand in the test set serves as a pivot point for alignment. The method requires a good choice of a highly active molecule to ensure efficiency and generate the best pharmacophore. In this study, the input was an arrangement of HIF-1α stabilizers known to bind to the 4W9H receptor protein. The primary input test set comprises the 18 ligand molecules of HIF-1α stabilizer interacting with 4W9H receptor protein were employed as the input query on the PharmaGist webserver to build a ligand-based best pharmacophore model. The pharmacophore discovery method then computes the output of pharmacophores using numerous flexible alignments of the input ligands. This approach quickly finds all candidate pharmacophores and reports the one with the highest score.[11]

2.2.1 Virtual screening. The obtained pharmacophore model was used as the 3D query for screening the ZINC purchasable database. ZINC is a comprehensive collection of commercially available, biologically relevant compounds suitable for screening. The ZINCPharmer library is synchronized with the ZINC library every month. Compounds are added and removed to maintain consistency and ensure that only currently purchasable compounds are retained. All screening experiments were performed using the online Zinc Pharmer database searching utility. Molecules with all the desired pharmacophore features were considered to be the hit molecules. The molecules successfully passed the initial tests. The selected molecules were subjected to molecular docking analysis.[12]

2.2.2 Molecular docking. PyRx 0.9 is used to investigate the activity in terms of binding affinity (kcal mol^{-1}), and then the outcomes are compared in binding affinity score for best-docked conformation. The structures of various HIF-1α stabilizers were drawn with the help of the Marvin sketch. A protein 4W9H was selected and downloaded from the protein data bank.[13] The human VHL (PDB id.4W9H) at a resolution of 2.10 Å (PDB).[14,15]

2.2.3 ADMET prediction. Among the numerous available computational tools for predicting the pharmacological properties and toxicological effects of chemical compounds on human health, we have selected the swissADME with an accuracy of a prediction usually higher than 70% and with friendly interfaces and tutorials available for free. We investigated the blood–brain barrier (BBB) penetration, XLOGP3, GI absorption, a CYP2D6 inhibitor, Lipinski, and the bioavailability of the proposed pyrazole derivatives. The PreADMET online bioinformatics tool was used to determine toxicity parameters such as mutagenicity, and toxicity levels of the chemicals were examined for diverse tissues.[16]

2.3 Synthesis

2.3.1 Synthesis of 2-benzoyl-3-phenyloxirane (1). In a 250 ml RBF, 7.28 g (0.035 M) of chalcone and 7 ml (0.3 M) of 30% aqueous H_2O_2 in 105 ml of ethanol were added. The temperature was maintained at 0–5 °C. Then, 2 ml of 5% NaOH was added to the mixture. The temperature was maintained for 15 h. Finally, the product was filtered and washed with water.[17]

2.3.2 Synthesis of 3,5-diphenyl-4,5-dihydro-1*H*-pyrazole-4-ol (2). In 250 ml RBF, 6 g (0.026 M) 3,5-diphenyl-4,5-dihydro-1*H*-pyrazol-4-ol was added, followed by 0.33 ml (0.042 M) hydrazine hydrate in 50 ml ethanol, which had previously produced. The reaction mixture was kept warm for 24 h under

reflux. With methanol, the residue was recovered and recrystallized.[18]

2.3.3 Synthesis of 3,5-diphenyl-1*H*-pyrazole (3). 5g (0.021 M) 3,5diphenyl-1*H*-pyrazole, 10 ml (0.166 M) acetic acid, and 1 ml H_2SO_4 were placed in a 250 ml RBF and agitated at room temperature for 6 h. After neutralizing the reaction mixture with NH_2OH solution and pouring it over crushed ice, the liquid was cooled. Filtration, water washing, and methanol crystallization were all used to prepare the final product.[17]

2.3.4 General procedure for the synthesis of pyrazole–Mannich bases (CDEA, CDIPA, CP, CI & CDPA). 0.01 M of step 3 product was added to 10 ml of ethanol. Then 0.01 M of respective secondary amines (imidazole/pyrazole/diethylamine/diisopropylamine/diphenyl amine) was added. Then the compound mixture was stirred at room temperature for 4 h. after that, 10 ml of water was added and kept at cold temperature overnight. Then the product was filtered and recrystallized with ethanol.[19]

2.3.5 Purification and analysis

2.3.5.1 1-(Imidazol-1-ylmethyl) −3,5-diphenylpyrazole [CI]. Yield–79%; color–white; Rf-0.36, Solvent System–petroleum ether : ethyl acetate (4 : 1); IR (cm^{-1}): 1074.16 (C–N str), 1569.77 (C=N str), 1673.91 (C=C str), 2855.1 (Ali C–H str), 3096.15 (Aro C–H str). ^{1}H NMR (400 MHz, $CDCl_3$) δ: 2.2 (s, 2H, N–CH_2), 7.2 (s, 1H, CH–pyrazole), 7.3–7.4 (m, 10H, Ar–H), 7.7 (s, 1H, CH–imidazole), 7.8 (d, 1H, CH–imidazole), 7.9 (d, 1H, CH–imidazole). ^{13}C NMR($CDCl_3$): (400 MHz, $CDCl_3$),108.34–130.81 (aromatic carbon)148.79 (pyrazole carbon). MS: 300 (M+).

2.3.5.2 3,5-Diphenyl-1-(pyrazole-1-ylmethyl) pyrazole [CP]. Yield–85%; color–white; Rf-0.52, Solvent System–petroleum ether : ethyl acetate (4 : 1); IR (cm^{-1}): 1074.16 (C–N str), 1569.77 (C=N str), 1604.48 (C=C str), 2855.1 (Ali C–H str), 3064.33 (Aro C–H str). ^{1}H NMR (400 MHz, $CDCl_3$) δ: 2.1 (s, 2H, N–CH_2), 7.3 (m, 10H, Ar–H), 7.5 (m, 3H, pyrazole–CH), 7.9 (s, 1H, pyrazole–CH). ^{13}C NMR (400 MHz, $CDCl_3$): 100–130 (aromatic carbon), 148.72 (pyrazole carbon). MS: 300 (M+).

2.3.5.3 N-[(3,5-diphenylpyrazol-1-yl) methyl] -N-phenylaniline [CDPA]. Yield–86%; color–white; Rf-0.21, Solvent System–petroleum ether : ethyl acetate (4 : 1); IR (cm^{-1}): 1074.16 (C–N str), 1594.84 (C=N str), 2857.02 (Ali C–H str), 3096.15 (Aro C–H str). ^{1}H NMR (400 MHz, $CDCl_3$) δ: 6.9 (s, 2H, N –CH_2), 7.2 (s, 1H, pyrazole–CH), 7.4 (m, 10H, Ar–H), 7.7 (m, 10H, Ar–H). ^{13}C NMR (400 MHz, $CDCl_3$): 18.44 (), 40.52 (C=C), 52.96, 58.49, 103.73–130.81 (aromatic carbon), 148.57 (pyrazole carbon). MS: 401 (M+).

2.3.5.4 (3,5-Diphenylpyrazol-1-yl) methyl] diethylamine [CDEA]. Yield–86%; color–white; Rf-0.42, Solvent System–petroleum ether : ethyl acetate (4 : 1); IR (cm^{-1}): 1074.16 (C–N str), 1570.74 (C=N str), 2856.06 (Ali C–H), 3096.15 (Aro C–H str), ^{1}H NMR (400 MHz, $CDCl_3$) δ: 1.2 (t, 6H, CH_3), 2.1 (s, 2H, N–CH_2), 6.6 (q, 4H, N–CH_2), 6.8 (s, 1H, pyrazole–CH), 7.6 (m, 10H, Ar). ^{13}C NMR (400 MHz, $CDCl_3$): 100.29–130.81 (aromatic carbon), 148.74 (pyrazole carbon).MS: *m*/*z* 305 (M+).

2.3.5.5 (3,5-Diphenylpyrazol-1-yl) methyl] diisopropylamine [CDIPA]. Yield–86%; color–white; Rf-0.64, Solvent System–petroleum ether : ethyl acetate (4 : 1); IR (cm^{-1}): 1074.16 (C–N str), 1587.13 (C=N str), 1604.48 (C=C str), 2856.06 (Ali C–H), 3096.15 (Aro C–H str). ^{1}H NMR (400 MHz, $CDCl_3$) δ: 1.2 (d, 12H, isopropyl – CH_3), 2.1 (s, 1H, pyrazole–CH), 3.8 (m, 2H, pyrazole–CH), 7.3 (m, 10H, Ar–CH_3). ^{13}C NMR (400 MHz, $CDCl_3$): 100.26–130.81 (aromatic carbon), 148.76 (pyrazole carbon) MS: 333 (M+).

2.4 *In vitro* studies

2.4.1 Mitochondrial synthesis determination by MTT assay. To assess cell viability, proliferation, and cytotoxicity, the MTT test is employed to quantify cellular metabolic activity on mouse embryo cell lines 3T3-L1. The percentage of cell viability was estimated using the following formula. The dose–response curves were used to create the concentrations of medication or test substances required to suppress cell growth by 50%.[20]

$$\%\ \text{cell viability} = \frac{\text{mean OD of individual sample}}{\text{mean OD control}} \times 100\%$$

2.4.2 Scratch wound assay. Basic cell migration parameters, including speed, persistence, and polarity can be easily measured using the scratch-wound test. Before inserting a narrow "wound" using a pipette tip, cells are grown to confluence. Wound healing begins at the wound's edge, where cells polarize and enter the wound space.[21]

2.5 *In vivo* studies

2.5.1 Acute oral toxicity study. The OECD 420 guideline was used during the research of acute oral toxicity. Each group of animals is given a set dose of 5, 50, 300, and 2000 mg kg^{-1} throughout the step-by-step procedure used in this study. A supplementary OECD Guidance Document describes clinical indications and conditions related to pain, suffering, and approaching death in detail. Other groups of animals may be dosed at greater or lesser fixed doses depending on the existence or absence of toxicity or death. This approach is repeated until the dose producing apparent toxicity is determined, until no effects are observed at the most significant dose, or until fatalities occur at the lowest dose.[22]

2.5.2 Grouping of animals. The animals were divided into three groups. Group 1 was given sterile gauze as a disease control, whereas groups 2 and 3 were given low and high doses. Institutional Animal Ethical Committee, JSS College of Pharmacy, Ooty. Approved all animal experiments. The study's IAEC number has been approved (JSSCP/OT/IAEC/23/2021-22). The formula was used to calculate the percentage of wound contraction.

$$\%\ \text{wound contraction} = \frac{A_0 - A}{A} \times 100$$

A_0: day 0 wound area. A_0: wound area on a particular day.

2.5.3 Induction of diabetes and full thickness excision wound model. Following a night of fasting, Wistar male albino rats weighing (200–220 g) (n = 24) were injected with a single intraperitoneal dosage of 55 mg kg^{-1} of freshly produced streptozotocin (STZ) in 0.1 M citrate buffer (pH 4.5). After 15 minutes, rats were given an intraperitoneal injection of 120 mg kg^{-1} nicotinamide (NAD). Rats were starved overnight after 96 hours, except for free access to water. Blood was drawn from the

tail vein of rats to assess fasting blood sugar levels with a glucometer. The injected rats were observed for 7 days, and those with blood glucose levels of more than 250 mg dl^{-1} are classified as type 2 diabetic. The animals were separated into three groups ($n = 6$).[23]

The wound healing effectiveness of synthesized compound **CI** was assessed using a full-thickness excision wound model. The animals were sedated with (75 mg kg^{-1} ketamine + xylazine 10 mg kg^{-1}, i.p.). Excision wounds with an area of 400 mm^2 and a depth of was created by removing a layer of skin from the shaved region. Until the therapy, the entire incision was kept exposed. Animals in groups III-IV will be given the test dosage orally. All groups' wound areas will be measured with a caliber on 0, 3, 6, 9, 12, 15 days.[24]

3 Results and discussion

3.1 *In silico* studies

3.1.1 Pharmacophore modelling. The spatial arrangement of attributes required for a drug to interact with a particular target receptor is known as a pharmacophore. These qualities are necessary for developing the optimal Pharmacophore Model. PharmaGist, a web server, generated the best ligand-based pharmacophore model. PharmaGist used the ligand-based pharmacophore detection approach. Only a Mol2 file containing drug-like compounds and an email address are necessary on the simplest input form. The chemical structures were obtained in SDF format from PubMed. The Open Babel GUI format converter tool was utilized to convert the format. Up to 18 molecules can now be stored in a single Mol2 file or multiple Mol2 files compacted into a single zip file. In a field on the basic form, we can specify the number of putative pharmacophores to report for each subset size of input molecules (5 by default). In the 'Advanced Options section of the form, we can choose additional attributes. These options are hidden by default, and changing them is optional. A website link that shows the best flexible alignment for every pair of input molecules discovered.

The generated pharmacophore was visualized by PyMOL software, which shows the physicochemical properties and the distance between any two properties. Finally, the best pharmacophore model was taken and pictured, as shown in Fig. 2. We obtained the pharmacophore containing two aromatic regions and one acceptor region.

3.1.2 Virtual screening. ZINCPharmer is a virtual screening tool for commercially accessible chemicals that runs on the web. Users can upload their molecules to a server and process them themselves. We anticipate that a large community of structural biologists and medicinal chemists will use this resource to create virtual screening libraries. Several filters in the ZINCPharmer application can be used to limit the database substances based on pharmacophoric features, such as: to reduce the number of conformer orientations returned, Max Hits per Conf is employed (due to varying mappings of query characteristics to ligand features). This filer is necessary for highly symmetric searches with infinite postures. Maximum hits per molecule: this setting limits the number of hits returned for the same molecule (in various conformations or poses). The priority sort order determines which effects are chosen. A number has been assigned to each molecule. Set a limit on the total number of hits that will be returned. The sort order entered in the result box determines which impacts are selected. Maximum RMSD: select the query features with the fewest RMSD and the molecule with the highest RMSD. RMSD's statistical significance: The forecast is usually successful if the RMSD is less than 2 Å. The goal is to make this "near-native" approach the most popular ligand position. As a result, we filtered the 153-Ligand in this study by producing the highest RMSD value, more than 0.42. Sort the Daltons by their molecular weight (value includes hydrogens). The 153-Ligand was filtered in this study by reducing the molecular eeight value to less than 500 Dalton. Rotatable bonds: sort by how many rotatable bonds there are. The SMARTS expression is used to identify rotatable bonds.

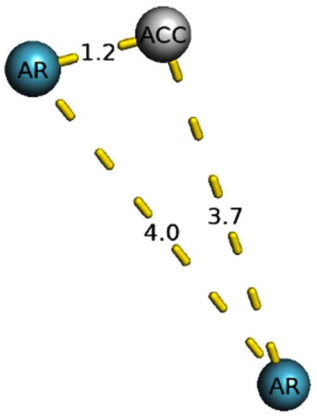

Fig. 2 Generated pharmacophore model.

The virtual screening was performed using the generated pharmacophore in ZINCPharmer shown in Fig. 3. For our research, we chose the natural product database. The PharmaGist's pharmacophore data is used to perform virtual screening. Based on the natural product database, ZINCPharmer generated 3782 hits. We chose 153 compounds based on their RMSD. According to ADMET, we decided on 20 compounds for docking investigations based on drug-likeness.

3.1.3 Molecular docking. Of all the chemicals tested, pyrazole analogues (**CI**, **CP**, **CDEA**, **CDPA**, **CDIPA**) had the highest

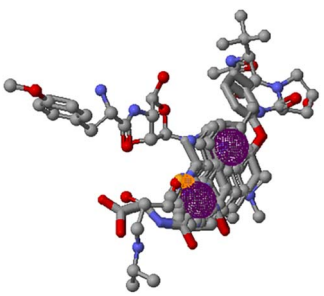

Fig. 3 Generated pharmacophore in ZINCPharmer.

binding affinity. The sci-finder novelty checks indicated that all five designed compounds were novel. PyRx virtual screening was used to dock the transformed pyrazole analogues against the VHL protein (PDB: 4W9H). Table 1 shows the 2D interactions of pyrazole analogues with VHL protein and these chemicals. The ADMET properties are given in Tables 2 and 3. The properties were in the acceptable range.

Table 1 Binding affinity and 2D interactions of designed pyrazole analogues

Compound code	Binding energy	2D Interaction
CI	−9.4	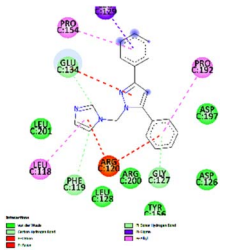
CP	−9.0	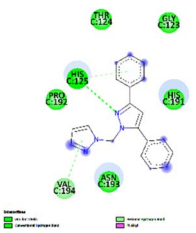
CDEA	−8.4	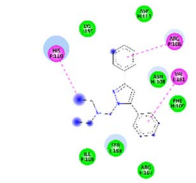
CDIPA	−8.1	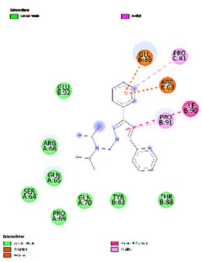
CDPA	−7.9	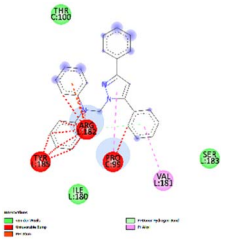
CO-CRYSTAL	−6.2	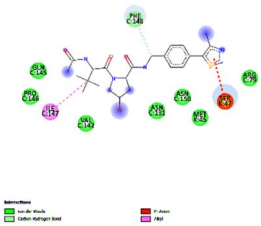

3.2 DMET studies

3.2.1 Synthesis of pyrazole analogues. The pyrazole analogues (**CI**, **CP**, **CDEA**, **CDPA**, **CDIPA**) were created because they had the best binding affinity and synthetic availability. Chalcone was epoxidized with hydrogen peroxide in an alkaline medium at 0 degrees Celsius. A heterocyclic molecule, 3,5-diphenyl-4-hydroxy-4,5-dihydro-1*H*-pyrazole, was synthesized using the Wharton reaction and epoxy chalcone (2a) generated without the use of acetic acid as a nucleophilic reagent using hydrazine hydrate (1.5–2 mol). Then 3,5-diphenyl-4-hydroxy-4,5-dihydro-1*H*-pyrazole thus formed was subjected to acid-catalysed dehydration to give the desired 3,5-diphenyl-1*H*-pyrazole. The 3,5-diphenyl-4-hydroxy-4,5-dihydro-1*H*-pyrazole was undergone a Mannich reaction to provide the final derivatives (**CI**, **CP**, **CDEA**, **CDPA**, **CDIPA**). TLC was used at every synthesis step to ensure it was completed. Petroleum ether : ethyl acetate (4 : 1) is the solvent system used for TLC.

3.3 *In vitro* studies

3.3.1 Mitochondrial synthesis determination by MTT assay. The cellular viability of the produced compounds was examined at various doses. Graphical correlation of percent viability with synthesized compound concentration g ml^{-1} was used to assess the data. For the MTT assay, the five inhibitors produced were identified as non-toxic. The IC_{50} value for these chemicals is shown in Table 4, and the percentage viability is depicted in Fig. 4.

3.3.2 Wound healing assay. The cell proliferation was measured using a wound healing test. After treatment, the cell migrations for the compound **CI** and **CP** were compared to other compounds. The wound width was measured at the moment of the scratch and again after 24 hours. The compounds affect 3T3-L1 cells' wound width control. All the compounds accelerated cell migration, which improved wound healing. The compounds **CI** and **CP** have shown comparable activity among the five compounds compared to the positive control hyaluronic acid, which is depicted in Fig. 4.

3.4 *In vivo* results

3.4.1 Acute oral toxicity studies. After doing acute oral toxicity trials, discovered that the groups receiving 5, 50, and 300 mg kg^{-1} of the test medication had no adverse effects or fatality. All the mice in the group receiving 2000 mg kg^{-1} of the test medication died. Based on these findings, we determined that 150 mg kg^{-1} was the high dose and 75 mg kg^{-1} was the low dose for pharmacological activity evaluation.

3.4.2 Evaluation of wound healing activity. Inflammation, granulation, and tissue remodelling are all involved in tissue repair and wound healing. In wound healing, cytokines and growth factors mediate interactions between various cells, extracellular matrix proteins, and their receptors. According to our research, compound (**CI**) improved wound healing in rats.

Table 2 ADME properties of designed compounds

Code	XLOG P3	GI absorption	BBB permeation	CYP2D6 inhibitor	Lipinski	Bio availability	Synthetic accessibility
CI	3.48	High	Yes	Yes	0	0.55	2.98
CP	3.7	High	Yes	Yes	0	0.55	3.03
CDEA	4.36	High	Yes	Yes	0	0.55	2.99
CDPA	6.96	Low	No	No	1	0.55	3.41
CDIPA	5.22	High	Yes	Yes	0	0.55	3.19

Table 3 Toxicity studies for designed compounds

Code	Algae test	Ames test	hERG inhibitor	TA1535_10RLI	TA1535_NA	Daphnia
CI	0.0001	Mutagen	Medium risk	Negative	Negative	0.005
CP	0.0002	Mutagen	Medium risk	Negative	Negative	0.011
CDEA	0.0002	Mutagen	Medium risk	Negative	Negative	0.016
CDPA	0.0002	Mutagen	Medium risk	Negative	Negative	0.010
CDIPA	0.0282	Mutagen	Medium risk	Negative	Negative	0.798832

Table 4 Percentage viability by MTT assay

Compound code	3T3-L1 IC_{50} μg ml^{-1}
CI	106.66
CP	111.37
CDEA	113.03
CDIPA	113.81
CDPA	131.70
Hyaluronic acid	112.59

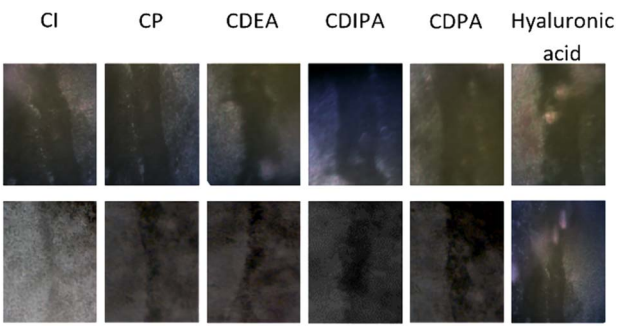

Fig. 4 Comparison of wound size in 0 h and 24 h.

Using a wound model, we assessed the oral therapeutic efficacy of (**CI**) on poor wound healing in diabetic rats. Animal wounds treated with compound (**CI**).

3.5 Wound contraction

Days 3, 7, 11, and 15 observed measurements of wound contraction, which are given in Table 5 as a percentage of the shrinkage of damaged areas in each group, as seen in Fig. 5. Table 5 lists the percentage of the reduction in the injured area. In this investigation, wounds treated with a (Group III) high dose (150 mg kg^{-1}) of compound **CI** contracted considerably faster than wounds treated with a (Group II) low dose of compound **CI** (75 mg kg^{-1}) and (Group I) disease control. After wound development, the mean percentage of wound contraction in the high dosage (150 mg kg^{-1}) treated group was substantially higher (81.02 ± 0.55% at day 15, $p < 0.001$) than in the disease control (41.26 ± 0.55% at day 15, $p < 0.01$) and low dose (53.210.55% at day 15, $p < 0.01$) groups.

4 Discussion

For efficient wound closure, we have adopted the technique of stabilizing HIF-1α levels in hyperglycaemic circumstances.

Table 5 Effect of test drug (CI) on wound contraction

	Wound contraction (%)			
Groups	Day 3	Day 7	Day 11	Day 15
Control	12.57 ± 0.55	15.50 ± 0.27	22.75 ± 0.28	39.9 ± 0.51
Low dose 75 mg kg^{-1}	18.25 ± 0.55*	24.50 ± 0.30*	41.5 ± 0.43*	55.77 ± 0.42**
High dose 150 mg kg^{-1}	24.5 ± 0.48*#	31.25 ± 0.39*#	64.00 ± 0.44*#	83.59 ± 0.60*#

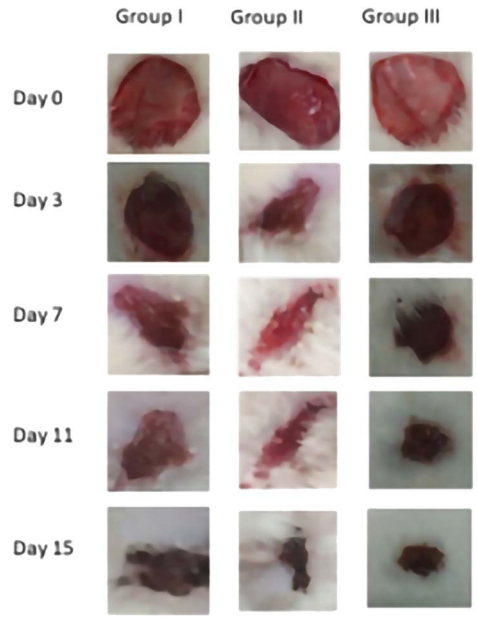

Fig. 5 Comparison of wounds at different intervals.

As shown in the Fig. 6, HIF-1α is directly involving in the major wound healing process such as increasing the level of VEGF and eNOS and also by decreasing the level of ROS levels. In normal condition HIF-1α binds with VHL which leads to the formation of proteasome, and is cleared from the body. By this mechanism HIF-1α is normally Salvaged. The stabilization of HIF-1α is done by mimicking the hypoxic conditions by making the synthesized compound bind with VHL in place of HIF-1α. Therefore, there will be abundant levels of HIF-1α and speeding up wound healing. Our core idea is to stabilize the HIF-1α levels by blocking the VHL and HIF-1α Interaction. Several studies discovered that small substances with drug-like potencies bind to "hotspots" on the contact surfaces involved in protein–protein interactions. Surprisingly, these small molecules bind to the target protein's contact surface more firmly and profoundly than the contact atoms of the native protein partner.[25] According to clinical research and the effectiveness of PHD inhibitors, HIF-1α signalling can be a therapeutic target for problems related to Angiogenesis. The hydroxylation of proline residues in the α-subunit of the hypoxia-inducible factor mediates the hypoxic response. PHD isozymes in humans, iron(II), and 2-oxogluta-rate dependent oxygenase catalyse hydroxylation.[26] The hydroxylation of HIF-1α is catalysed by prolyl-4-hydroxylases belonging to the superfamily of Fe(II) and 2-oxoglutarate (2-OG) dependent and related oxy-geneses, as was discovered using a chemical genetics approach. Three enzymes known as PHD1-3, or PHD enzymes, have been discovered in humans.[27] Becaplermin, a recombinant platelet-derived growth factor-BB (rhPDGF-BB), was the first FDA-approved wound healing product. The FDA has approved bio-engineered skin-care products such as Apligraf and Dermagraft for treating diabetic foot ulcers (DFU).[28] FG-2216 is in clinical trials (IOX3), an effective and orally active inhibitor of HIF-1α prolyl hydroxylase-2 (PHD2) with an IC50 of 3.9 M. *In vivo*, FG-2216 produces high levels of erythropoietin and low levels of haemoglobin.[29]

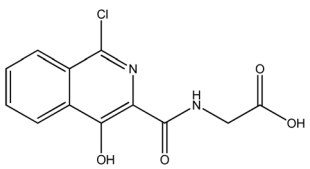

FG-2216

Previous research has demonstrated that hyperglycaemia inhibits HIF-1α's activity in diabetic mice by destabilizing it through a VHL-dependent mechanism. Therefore, inhibiting upstream PHDs is a potentially inferior technique to stabilizing HIF-1α *via* preventing the down–stream interaction of HIF-1α and VHL from preventing HIF-1α independent off-target consequences, as have been noted with PHD inhibitors in clinical development. In this context, interrupting the VHL–HIF-1α PPI may be a highly effective strategy for treating diabetic wounds.[4] Only VH298 has been found to stimulate wound healing and enthesis healing *in vivo*, and few inhibitors of the interaction between VHL and HIF-1α have been discovered to date. To confirm that the increase in HIF-1α was prompted by the inhibition of VHL activity, clear cell renal cell carcinoma A498 cells, which lack functional VHL, were treated with VH298, a potent inhibitor of the VHL–HIF–1 PPI. The PHD inhibitor FG-4592 was also used as a control compound.[25]

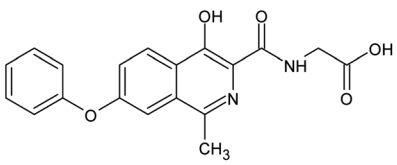

FG-4592

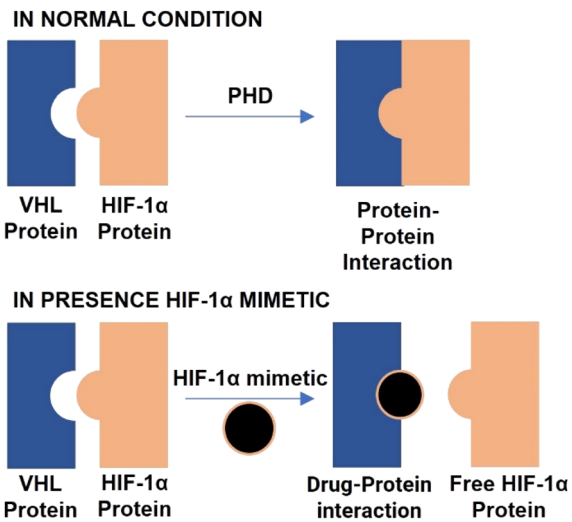

Fig. 6 Mechanism of HIF-1α stabilizer.

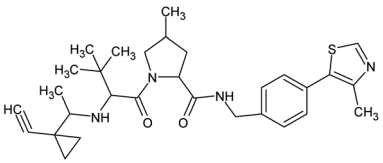

VH-298

Due to their high structural diversity and easily tuneable steric and electronic properties, metal complexes can take on various geometrical shapes depending on the oxidation state of their metal centres and the nature of their co-ligands.[25] Some metal complexes have become adaptable drug discovery scaffolds. In that study, the first metal-based inhibitor of the VHL–HIF–1α interaction was described as an Ir(III) metal complex.

4.1 Ir(III) metal complex

As a result of their easily changeable reactivity (from prone to inert), high water solubility, inertness to air, and synthetic accessibility, metal complexes have become functional scaffolds for drug development or bioanalysis.[29] Metal compounds have distinctive yet adjustable characteristics, such as their electrical properties, chemical reactivities, and molecular structures, which allow them to adopt three-dimensional geometries that can explore as yet undiscovered hotspots of the protein binding site.[25]

Ir III complex demonstrated encouraging wound healing activity in this type 2 diabetes model when injected intraperitoneally. Additionally, the complex was administered topically to db/db mice, a commonly used diabetes model, to demonstrate that our substance might also hasten wound closure when applied topically. Although the binding affinity of the complex is about 100 times lower than that of the currently available VHL–HIF–1α inhibitor VH298, Administering Ir III complex at higher dosages (over 30 times greater than the dosage of VH298 used in a previous study) and through different routes can lead to a significant accumulation of complex at injured skin tissue and promising wound healing effects in animal models of diabetes.[30,31]

In this backdrop, an alternative finding of existing HIF-1α stabilizers, we have carried out a systematic *in silico* followed by *in vitro* and *in vivo* studies. At the end of the study, a new class of HIF-1α stabilizers was created as an alternative to conventional PHD inhibitors. Five novel pyrazole analogues (**CI**, **CP**, **CDEA**, **CDPA**, **CDIPA**) are developed at the end of this study as HIF-1α memetics Scheme 1.

We propose the following structural features for diabetic wound healing therapy through the HIF-1α memetic pathway.

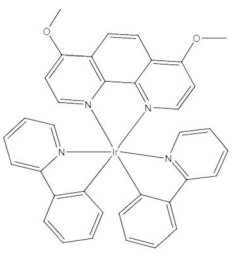

Ir(III) metal complex

Step1 Synthesis of 2-benzoyl-3-phenyloxirane (1)

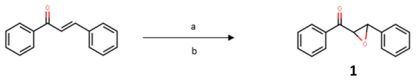

Reagents and conditions

a) 30% Hydrogen peroxide (H_2O_2), Sodium Hydroxide (NaOH).
b) Ethanol (C_2H_5OH), reflux 15 h.

Step 2 Synthesis of 3,5-diphenyl-4,5-dihydro-1H-pyrazole-4-ol (2)

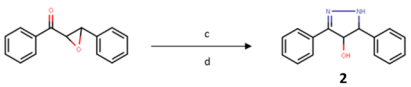

Reagents and conditions

c) Hydrazine hydrate (NH_2-NH_2).
d) Ethanol (C_2H_5OH), reflux 15 h.

Step 3 Synthesis of 3,5-diphenyl-1H-pyrazole (3)

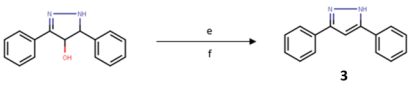

Reagents and conditions

e) Acetic acid (CH_3-COOH), Sulfuric acid (H_2SO_4).
f) Ethanol (C_2H_5OH), Stir at room temperature for 15 h.

Step 4 Synthesis of Pyrazole -Mannich bases (CDEA, CDIPA, CP, CI &CDPA)

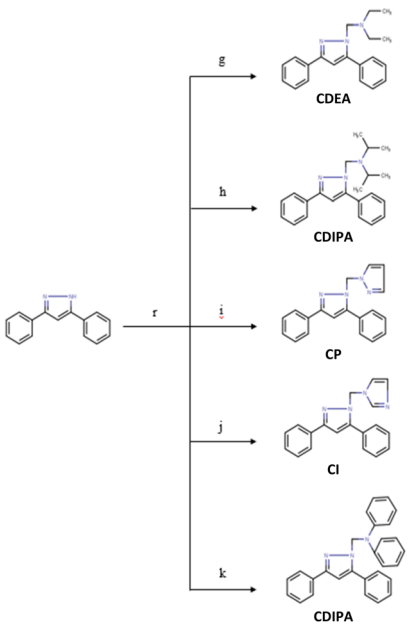

Reagents and conditions

g) Diethylamine
h) Diisopropylamine
i) Pyrazole
j) Imidazole
r) Diphenylamine Formaldehyde (HCHO), Stir at room temperature for 4h.

Scheme 1

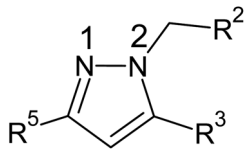

(1) Presence of pyrazole nucleus.
(2) Substitution of unsubstituted phenyl rings at R_3 and R_5
(3) Substitution of five-membered azole ring such as pyrazole and imidazole through a methylene linkage at N_2 position.

5 Summary and conclusion

Small bioactive compounds are the focus of the current study because there is an urgent need to speed up research in this field to find treatments and cures for diabetic wound healing. HIF-1α signalling can be a pharmacological target for disorders associated with angiogenesis, as shown in clinical trials by the efficiency of PHD inhibitors. However, PhD inhibitors have a few drawbacks, such as a lack of target specificity and potentially harmful side effects. There were aberrant liver enzyme test results in a Phase 2 trial with FG-2216, and one patient died of hepatic necrosis. A new class of HIF-1α stabilizers has been created as an alternative to conventional PHD inhibitors. Five novel pyrazole analogues (**CI, CP, CDEA, CDPA, CDIPA**) are developed at the end of this study as HIF-1α memetics. Two new small molecule HIF-1α stabilizers are future therapeutics for wound repair, and our investigation verifies the potential of healing diabetic wounds by inhibiting the interaction between VHL and HIF-1α.

Conflicts of interest

The author declares that there are no conflicts of interest.

Acknowledgements

The authors are thankful to the JSS College of Pharmacy, Ooty, for providing the necessary facilities for research.

References

1 *Metalloproteinases and their inhibitors: Regulators of wound healing-ScienceDirect*, 2022, available from: **https://www.sciencedirect.com/science/article/abs/pii/S1357272507003433**.
2 *HIF-1 is expressed in normoxic tissue and displays an organ-specific regulation under systemic hypoxia-STROKA-2001*, The FASEB Journal-Wiley Online Library, 2022, available from: **https://faseb.onlinelibrary.wiley.com/doi/full/10.1096/fj.01-0125com**.
3 *LW6, a novel HIF-1 inhibitor, promotes proteasomal degradation of HIF-1α via upregulation of VHL in a colon cancer cell line-ScienceDirect*, 2022, available from: **https://www.sciencedirect.com/science/article/abs/pii/S0006295210004521**.
4 *Stabilization of HIF-1α is critical to improving wound healing in diabetic mice|PNAS*, 2022, available from: **https://www.pnas.org/doi/abs/10.1073/pnas.0805230105**.
5 *Reaching for high-hanging fruit in drug discovery at protein-protein interfaces|Nature*, 2022, available from: **https://www.nature.com/articles/nature06526**.
6 J. A. Wells and C. L. McClendon, Reaching for high-hanging fruit in drug discovery at protein-protein interfaces, *Nature*, 2007, **450**(7172), 1001–1009.
7 J. Frost, C. Galdeano, P. Soares, M. S. Gadd, K. M. Grzes, L. Ellis, *et al.*, Potent and selective chemical probe of hypoxic signalling downstream of HIF-α hydroxylation via VHL inhibition, *Nat. Commun.*, 2016, **7**(1), 1–12.
8 *The Role of Oxidative Stress and Antioxidants in Diabetic Wound Healing*, 2022, available from: **https://www.hindawi.com/journals/omcl/2021/8852759/**.
9 *HIF1α overexpression enhances diabetic wound closure in high glucose and low oxygen conditions by promoting adipose-derived stem cell paracrine function and survival|Stem Cell Research & Therapy|Full Text*, 2022, available from: **https://stemcellres.biomedcentral.com/articles/10.1186/s13287-020-01654-2**.
10 *Arnebin-1 promotes Angiogenesis by inducing eNOS, VEGF and HIF-1α expression through the PI3K-dependent pathway*, 2022, available from: **https://www.spandidos-publications.com/ijmm/36/3/685**.
11 M. T. Muhammed and A. Y. Esin, Pharmacophore Modeling in Drug Discovery: Methodology and Current Status, *J. Turk. Chem. Soc., Sect. A*, 2021, **8**(3), 749–762.
12 A. Good, Structure-based virtual screening protocols, *Curr. Opin. Drug Discov. Dev*, 2001, **4**(3), 301–307.
13 T. P. O'Sullivan and G. C. Hargaden, Flexible, online teaching and assessment of organic chemistry using MarvinSketch and SMILES, *5th Eurovariety in Chemistry Education 2013, Abstract book*, University of Limerick, Limerick, Ireland, 2013.
14 N. Guex and M. C. Peitsch, SWISS-MODEL and the Swiss-Pdb Viewer: an environment for comparative protein modeling, *Electrophoresis*, 1997, **18**(15), 2714–2723.
15 R. P. Pawar and S. H. Rohane, Role of autodock vina in PyRx molecular docking, *Asian J. Res. Chem.*, 2021, **14**(2), 132–134.
16 A. Daina, O. Michielin and V. Zoete, SwissADME: a free web tool to evaluate pharmacokinetics, drug-likeness and medicinal chemistry friendliness of small molecules, *Sci. Rep.*, 2017, **7**(1), 1–13.
17 B. A. Bhat, S. C. Puri, M. A. Quraishi, K. L. Dhar and G. N. Qazi, Synthesis of 3,5-diphenyl-1*H*-pyrazoles, *Synth. Commun.*, 2005, **35**(8), 1135–1142.
18 K. Karrouchi, S. Radi, Y. Ramli, J. Taoufik, Y. N. Mabkhot, F. A. Al-Aizari, *et al.*, Synthesis and pharmacological activities of pyrazole derivatives: A review, *Molecules*, 2018, **23**(1), 134.
19 S. Viveka, P. Shama, G. K. Nagaraja, N. Deepa and M. Y. Sreenivasa, Design, synthesis, and pharmacological studies of some new Mannich bases and S-alkylated analogs of pyrazole integrated 1, 3, 4-oxadiazole, *Res. Chem. Intermed.*, 2016, **42**(3), 2597–2617.

20 J. V. Meerloo, G. J. Kaspers and J. Cloos, Cell sensitivity assays: the MTT assay, in *Cancer cell culture*, Springer, 2011, p. 237–245.
21 C. C. Liang, A. Y. Park and J. L. Guan, In vitro scratch assay: a convenient and inexpensive method for analysis of cell migration in vitro, *Nat. Protoc.*, 2007, **2**(2), 329–333.
22 L. Worasuttayangkurn, W. Nakareangrit, J. Kwangjai, P. Sritangos, N. Pholphana, P. Watcharasit, *et al.*, Acute oral toxicity evaluation of Andrographis paniculata-standardized first true leaf ethanolic extract, *Toxicol Rep.*, 2019, **6**, 426–430.
23 A. Ghasemi, S. Khalifa and S. Jedi, Streptozotocin-nicotinamide-induced rat model of type 2 diabetes, *Acta Physiol. Hung.*, 2014, **101**(4), 408–420.
24 E. Pişkin, İ. A. İşoğlu, N. Bölgen, I. Vergel, S. Griffiths, T. Çavuşoğlu, *et al.*, In vivo performance of simvastatin-loaded electrospun spiral-wound polycaprolactone scaffolds in reconstruction of cranial bone defects in the rat model, *J. Biomed. Mater. Res., Part A*, 2009, **90**(4), 1137–1151.
25 G. Li, C. N. Ko, D. Li, C. Yang, W. Wang, G. J. Yang, *et al.*, A small molecule HIF-1α stabilizer that accelerates diabetic wound healing, *Nat. Commun.*, 2021, **12**(1), 1–11.
26 V. H. Haase, HIF-prolyl hydroxylases as therapeutic targets in erythropoiesis and iron metabolism, *Hemodial. Int.*, 2017, **21**(1), S110–S124.
27 M. J. Strowitzki, E. P. Cummins and C. T. Taylor, Protein Hydroxylation by Hypoxia-Inducible Factor (HIF) Hydroxylases: Unique or Ubiquitous?, *Cells*, 2019, **8**(5), 384.
28 G. Li, D. Li, C. Wu, S. Li, F. Chen, P. Li, *et al.*, Homocysteine-targeting compounds as a new treatment strategy for diabetic wounds via inhibition of the histone methyltransferase SET7/9, *Exp. Mol. Med.*, 2022, **54**(7), 988.
29 V. H. Haase, Hypoxia-inducible factor–prolyl hydroxylase inhibitors in the treatment of anemia of chronic kidney disease, *Kidney Int. Suppl.*, 2021, **11**(1), 8–25.
30 C. H. Leung, S. Lin, H. J. Zhong and D. L. Ma, Metal complexes as potential modulators of inflammatory and autoimmune responses, *Chem. Sci.*, 2015, **6**(2), 871–884.
31 D. Li, C. Peng, X. Xie, Y. Mao, M. Li, Z. Cao, *et al.*, Antidiabetic effect of flavonoids from Malus toringoides (Rehd.) Hughes leaves in diabetic mice and rats, *J. Ethnopharmacol.*, 2014, **153**(3), 561–567.